Technique for simple apatite coating on a dental resin composite with light-curing through a micro-rough apatite layer

Yasushi Hibino[a, b,*], Ayako Oyane[a,*], Kanako Shitomi[c], Hirofumi Miyaji[c]

[a] *Nanomaterials Research Institute, National Institute of Advanced Industrial Science and Technology (AIST), Central 5, 1-1-1 Higashi, Tsukuba, Ibaraki, 305-8565, Japan*

[b] *Division of Dental Biomaterials Science, Department of Restorative and Biomaterials Sciences, School of Dentistry, Meikai University, 1-1, Keyakidai, Sakado, Saitama, 350-0283, Japan*

[c] *Department of Periodontology and Endodontology, Faculty of Dental Medicine, Hokkaido University, N13W7, Kita-ku, Sapporo, Hokkaido, 060-8586, Japan*

* Corresponding authors:
Yasushi Hibino, DDS, PhD,
Nanomaterials Research Institute, National Institute of Advanced Industrial Science and Technology (AIST)
Address: Central 5, 1-1-1 Higashi, Tsukuba, Ibaraki 305-8565, Japan

Division of Dental Biomaterials Science, Department of Restorative and Biomaterials Sciences, School of Dentistry, Meikai University
E-mail: hibino@dent.meikai.ac.jp, Tel: +81-49-279-2761, Fax: +81-49-287-8260
Address: 1-1, Keyakidai, Sakado, Saitama 350-0283, Japan

Ayako Oyane, PhD, Nanomaterials Research Institute, National Institute of Advanced Industrial Science and Technology (AIST)
E-mail: a-oyane@aist.go.jp, Tel: +81-29-861-3005, Fax: +81-29-861-3005
Address: Central 5, 1-1-1 Higashi, Tsukuba, Ibaraki 305-8565, Japan

Abstract

Tooth root surfaces restored with dental resin composites exhibit inferior biocompatibility. The objective of this study was to develop a simple technique for coating apatite onto a resin composite to improve its surface biocompatibility. First, we fabricated a polymer film coated with a micro-rough apatite layer and pressed it (coating-side down) onto a viscous resin composite precursor. As a result of light-induced curing of the precursor through the overlaid film, the micro-rough apatite layer was integrated with the resin composite and, thus, transferred from the polyethylene terephthalate film surface to the cured resin composite surface as a result of the difference in interfacial adhesion strength. The transferred apatite layer attached directly to the cured resin composite without any gaps at the microscopic level. The adhesion between the apatite layer and the cured resin composite was so strong that the layer was not peeled off even by a tape-detaching test. The flexural strength of the resulting apatite-coated resin composite was comparable to that of the clinically used resin composite while satisfying the ISO requirement for polymer-based restorative materials. Furthermore, the apatite-coated resin composite showed better cell compatibility than the uncoated resin composite. The present apatite coating technique is well suited for dental treatment because the coating is applied during a conventional light curing procedure through simple utilization of the apatite-coated polymer film in place of an uncoated film. The proposed technique represents a practical evolution in dental treatment using light-curing resin composites, although further *in vitro* and *in vivo* studies are needed.

Key words: apatite, resin composite, dental resin, coating, interface, biocompatibility

1. Introduction

Dental resin composites composed of an organic polymer matrix and inorganic ceramic fillers have long been used in dental practice [1]. Because of recent advancements in their mechanical, chemical, and aesthetic properties, dental resin composites have been increasingly used not only in indirect restorations as adhesive materials but also in direct restorations. In direct restorations, resin composites have been used as restorative materials for occlusal caries, root caries, and root perforation and resorptions, as core build-up materials, and as pit and fissure sealants. In direct restorations, resin composites are generally prepared during treatments via light-induced polymerization. First, a viscous resin composite precursor composed of acrylate-based monomers, ceramic fillers, and additives is injected into a tooth cavity. The precursor filled into the cavity is pressed and shaped with a filling instrument for occlusal restoration, or a transparent polymer film (referred to as a dental strip) or cup for interproximal and cervical restoration. A curing light is used to irradiate the precursor to polymerize the monomers, thereby transforming the viscous precursor into a hard resin composite with an intended shape at a required region.

For certain applications such as the restoration of severe root caries and the repair of root perforations, a portion of the cured resin composite is exposed on the root surface and contacts the surrounding periodontal tissues, *i.e.*, gingival and alveolar bone tissues. However, resin composites lack in cementogenesis and usually exhibit inferior biocompatibility as compared with the natural root surface (they are likely to form fibrous tissues on their surfaces [2]). Thus, the exposed resin composite surface can cause widening of the periodontal ligament space, a reduction of occlusal support, and an increase of infection risk because of the epithelial downgrowth and attachment loss [3].

Numerous efforts have been made to produce resin composites with antibacterial property and/or improved biocompatibility [4]. For example, antibacterial monomers [5-7] and fillers [8-10] have been utilized to produce antibacterial resin composites. Biofunctional components such as osteoconductive fillers [11, 12], fillers containing osteogenic elements [13], and polymeric particles containing growth factors [14], have been utilized to produce resin composites with better biocompatibility.

In conventional approaches described above, resin composites have been functionalized by modifying their components (monomers, fillers, etc.). Recently, Nathanael *et al* proposed another approach based on surface functionalization of cured resin composites through apatite coating [15]. In their technique, the surface of a cured resin composite was coated with apatite *via* pulsed laser irradiation in a supersaturated calcium phosphate (CaP) solution. Apatite is a biomineral found in human bones and teeth (98 mass % in enamel, 72 mass % in dentin, and 65 mass % in cementum) [16]. Apatite [more specifically, hydroxyapatite: $Ca_{10}(PO_4)_6(OH)_2$] exhibits good biocompatibility and osteoconductivity; hence, it has long been used as implantable biomaterials [16,17]. In dental practice, apatite-coated metallic implants have been widely used. This is because apatite layers coated on dental implants are capable of enhancing osseointegration of the implants [16,17]. In addition, there are some recent reports suggesting the beneficial effects of apatite on periodontal regeneration [18-20]. For instance, Mao *et al* reported that apatite with a specific nano/micro structure enhanced osteogenic and cementogenic differentiation of human periodontal ligament stem cells [18]. Kano *et al* reported that apatite-coated implants regenerated the periodontal ligament-like tissue under the occlusal loading condition in rats [19]. Oshima *et al* reported that apatite-coated implants combined with dental follicle stem cells regenerated periodontal tissues including

periodontal ligament and cementum in mice [20]. Based on these backgrounds, apatite-coated resin composites are expected to demonstrate superior biocompatibility to the uncoated ones, thereby offering clinical benefits to restored root surfaces.

Although there are various apatite coating techniques, such as plasma spraying, sputtering, pulsed laser deposition, and biomimetic processes [16,17], few techniques meet the requirements (e.g., facileness and coating-area specificity) for chair-side apatite coating of a restored root surface. Even with the Nathanael's coating technique applied to resin composites [15], an additional laser irradiation step is required after the resin curing step. The purpose of the present study is to establish a simple apatite coating technique for a dental resin composite, where the coating is applied simultaneously with light curing. The technique is designed to be available during a conventional procedure without increasing the treatment time or number of steps. We hypothesized that, if the curing light is passed through an apatite-coated polymer film, the resulting cured resin composite should be coated with an apatite layer as a result of apatite transfer from the film.

To ensure sufficient apatite–resin attachment, we fabricated a micro-rough apatite coating layer on a polymer film via a precursor-assisted biomimetic process [21, 22], anticipating a mechanical interlocking effect. In the precursor-assisted biomimetic process, a polymer substrate is precoated with nanoparticulate amorphous CaP (precursor of apatite) by alternate dipping operations in calcium and phosphate ion solutions, and then immersed in a supersaturated CaP solution for a certain period. During the immersion step, nanoparticulate amorphous CaP on the substrate grows into a continuous layer of nano/micro-structured apatite. In this study, an apatite-coated polymer film (or an uncoated film as a control) was placed over a resin composite precursor, and the precursor was cured by photopolymerization. The surface structure, flexural strength, and cell

compatibility of the thus-obtained resin composites were examined.

2. Materials and Methods

2.1 Preparation of PET films

As the polymer film, we used a transparent and flexible polyethylene terephthalate (PET) film (Teijin Tetoron Film, Teijin Film Solutions Ltd., Tokyo, Japan) with a thickness of 23 μm. The PET film was cut into 2.5 mm × 30 mm rectangles (for rectangular specimens) or 10 mm × 10 mm squares (for disk-shaped specimens). The PET films were washed ultrasonically with ethanol, dried under vacuum at 100 °C for 24 h, and stored in a desiccator before use in subsequent experiments.

2.2 Preparation of apatite-coated PET films

A supersaturated CaP solution (CP solution) was prepared using reagent-grade chemicals (all from Nacalai Tesque, Inc., Japan) according to the protocol described elsewhere [15, 23]. Briefly, NaCl (142 mM), $K_2HPO_4 \cdot 3H_2O$ (1.50 mM), HCl (40 mM), and $CaCl_2$ (3.75 mM) were dissolved in ultrapure water, and the final solution pH was adjusted to 7.40 at 25.0°C by adding tris(hydroxymethyl)aminomethane (50 mM) and 1 M HCl (as necessary for pH adjustment) slowly to the solution. The as-prepared CP solution was tightly sealed in a polystyrene bottle and stored at 4°C before use in the following experiments.

The PET film prepared as described in Section 2.1 was coated with a micro-rough apatite layer by a precursor-assisted biomimetic process [21, 22]. First, the PET film was treated with oxygen gas plasma using a compact ion etcher (FA-1, SAMCO Inc., Kyoto, Japan) at an O_2 gas pressure of 30 Pa and a plasma power density of 1.0 W/cm^2 under an

electric field operating at 13.56 MHz for 30 s. The plasma-treated PET film was dipped into 20 mL of a 50:50 (in vol%) mixture of ethanol and 200 mM $CaCl_2$ for 10 s, then dipped into 20 mL of 50 vol% aqueous ethanol for 1 s and dried in air for 5 min. The substrate was subsequently dipped in 20 mL of a 50:50 (in vol%) mixture of ethanol and 200 mM $K_2HPO_4 \cdot 3H_2O$ for 10 s, dipped again in 20 mL of 50 vol% aqueous ethanol for 1 s, and dried in air for 5 min. These alternate dipping operations in calcium and phosphate ion solutions were repeated three times to precoat the PET film with CaP. The dipping and withdrawal rate was fixed at 50 cm/min with the use of a linear head motor equipped with a speed controller (Oriental Motor Co., Ltd., Japan). The CaP-precoated PET film was subsequently immersed in 3 mL of the CP solution at 25°C for 24 h to form a micro-rough apatite layer on its surface. After immersion, the film was removed from the solution, gently washed with ultrapure water, and air-dried.

2.3 Sample preparation: Light curing of the resin composite

Using the uncoated and apatite-coated polymer films, we prepared resin composite specimens (referred to as Samples RC and A-RC, respectively) by the experimental scheme shown in Figure 1. For both samples, w~~W~~e prepared two types of specimens: disk-shaped specimens (1.6 mm in thickness, 5 mm in diameter) and rectangular specimens (2.0 ± 0.1 mm in thickness, 2.0 ± 0.1 mm × 25 ± 0.2 mm in dimension). Rectangular specimens were used for the flexural strength measurement in Section 2.6, whereas disk-shaped specimens were used for all other experiments described in Sections 2.4, 2.5, and 2.7. As a resin composite, we used a clinically approved light-cured resin composite (GRACEFIL Flo A3; GC Inc., Tokyo, Japan) prepared from a low-viscosity precursor composed of 30 mass% acrylate-based monomers and 70 mass% SiO_2–BaO-

based ceramic fillers (~0.7 μm in diameter). The acrylate-based monomers are 2,2-bis-[4-(2-methacryloxyethoxy) phenyl] propane (Bis-MEPP), urethane dimethacrylate (UDMA), and triethyleneglycol dimethacrylate (TEGDMA).

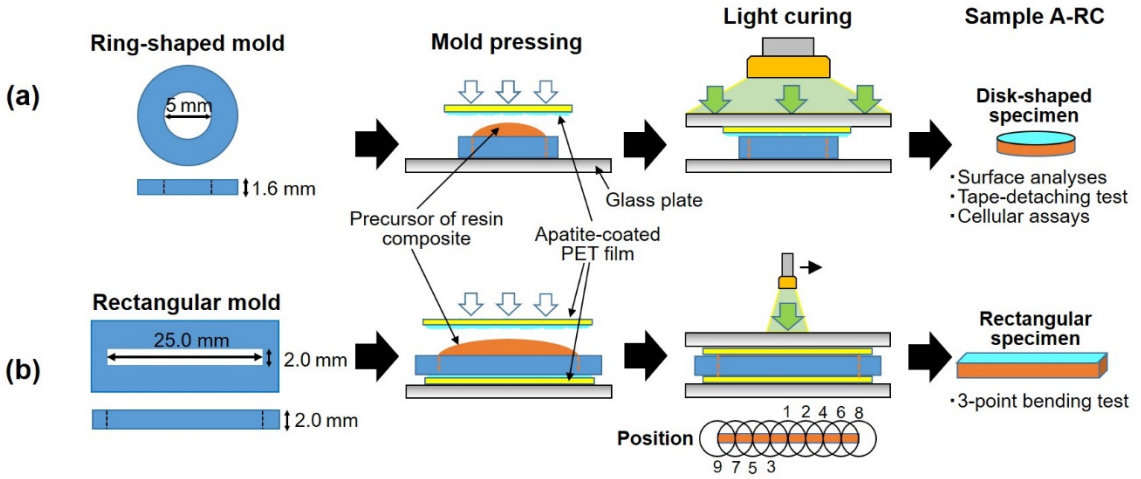

Fig. 1 Preparation scheme of the (a) disk-shaped and (b) rectangular specimens of Sample A-RC using apatite-coated polymer films. Specimens of Sample RC were prepared by the same scheme using uncoated films.

Disk-shaped specimens were prepared using square PET films and ring-shaped metal molds (1.6 mm in height, 5.0 mm in inner diameter), as shown in Figure 1 (upper row). First, the mold was placed on the uncoated PET film on a slide glass. The precursor of the resin composite was injected into the mold to fill the cavity according to the manufacturer's protocol. The apatite-coated PET film (apatite-coated surface down) or uncoated PET film as a control was placed over the precursor-filled mold and hand-pressed with another glass plate on it. The precursor was irradiated with blue LED light ($380 \leq \lambda \leq 430$ nm, 1 W/cm^2) for 10 s through the PET film using a dental curing light (PenCure, J. Morita Corp., Japan). After the light-induced curing process, the resin

composite was removed from the mold and the PET film was removed from the cured resin composite surface. The light-irradiated topside surfaces of the specimens (apatite-coated surface in Sample A-RC) were used in the following experiments unless otherwise specified.

Rectangular specimens were prepared using the rectangular PET films and rectangular stainless streel molds (2.0 ± 0.1 mm in height, 2.0 ± 0.1 mm × 25 ± 0.2 mm in inner dimension) according to International Organization for Standardization (ISO) standard 4049 (Dentistry-Polymer-based restorative materials) [24], as shown in Figure 1 (lower row). The mold was placed on the apatite-coated PET film (apatite-coated surface up) or uncoated PET film as a control on a slide glass. The resin composite precursor was injected into the mold to fill the cavity according to the manufacturer's protocol. The apatite-coated PET film (apatite-coated surface down) or uncoated PET film as a control was placed over the precursor-filled mold and hand-pressed using another glass plate. The dental curing light was used to irradiate the precursor with blue LED light from its top and bottom sides, through the PET films. Each side surface was entirely light-irradiated through step-by-step relocation of the irradiated region from Position 1 to 9, as outlined in the last step in Figure 1 (lower row).

2.4 Surface analyses

The surfaces of the apatite-coated PET film and Samples RC and A-RC (disk-shaped specimen) were analyzed by scanning electron microscopy (SEM, TM 4000 Plus, Hitachi High-Technologies Corp., Japan) in conjunction with energy-dispersive X-ray spectroscopy (EDX; AZtec One, Oxford Instruments, UK). Prior to the SEM and EDX analyses, the specimen surfaces were coated with a thin Au layer using a sputter coater

(SC-701 Mk II, Sanyu Electron Inc., Japan). The crystal structures of the surfaces of the uncoated and apatite-coated PET films and Samples RC and A-RC were analyzed by thin-film X-ray diffraction (XRD; Ultima IV and Ultima III, Rigaku Co., Japan) with CuKα radiation. The backside surfaces (central region) of Samples RC and A-RC (4 hours after preparation) were analyzed by Fourier transform infrared (FT-IR) spectroscopy (FT/IR-4700, JASCO Corporation, Japan) equipped with an attenuated total reflection (ATR) accessory with a monolithic diamond crystal. Three specimens were tested for each sample to confirm reproducibility.

A cross section of Sample A-RC (disk-shaped specimen) was further analyzed using a conventional resin embedding method. First, the specimen was covered with Si plates on both sides, embedded in an epoxy resin precursor and cured at 80°C. A cross-sectional specimen was prepared from the cured resin using a slow-speed diamond saw. The sectioned surface was polished with diamond powder (diameter: 15 μm → 9 μm → 3 μm) and finished by Ar^+-ion-beam milling using an ion milling system (E-3500, Hitachi High-Technologies Corp., Japan). The cross-sectional specimen was then sputter-coated with Au and used for the SEM and EDX analyses. In the cross-sectional SEM image, thickness of the apatite layer was measured at 10 different regions to calculate the mean and standard deviation.

2.5 Tape-detaching test

The disk-shaped specimen of Sample A-RC was subjected to a tape-detaching test [25] for preliminary assay of the coating adhesion. An acrylic-based tape (Scotch® 243J, 3M Company, USA) with nominal adhesion of 1.06 N/cm (180° peel test) was attached to half of the specimen surface and subsequently removed. Both the tape-detached and

intact surfaces were examined by SEM and EDX.

2.6 Flexural strength measurements

The rectangular specimens of Samples RC (control) and A-RC were stored in a desiccator at 25°C for 24 h after preparation (Section 2.3) and subjected to the three-point bending test in accordance with ISO 4049 [24]. The specimen was placed on supporting rods (2.0 mm in diameter, 20.0 mm in span-length) of the three-point bending jig. A universal testing machine (STB-1225S, A&D Inc., Japan) was used to apply a compressive load to the specimen in air at 23 ± 2°C via a loading rod (2.0 mm in diameter) at a crosshead speed of 1.0 mm/min until fracture occurred.

The flexural strength δ (MPa) of each specimen was calculated from the measured fracture load P (N) using equation (1):

$$\delta = 3Pl/(2wb^2) \quad (1)$$

where l is the span length (20.0 mm) between the supporting rods and w and b are the width (~2.0 mm) and thickness (~2.0 mm) of the specimen. The w and b values for each specimen were measured with a digital micrometer (MDC-25PX, Mitutoyo Corp., Japan) prior to the test. Six specimens were tested for each sample. The results were analyzed using Student's t-test, and $p < 0.05$ was considered statistically significant.

2.7 Cell compatibility assay

To evaluate cell compatibility of Sample A-RC, we performed cell proliferation assay, actin staining, and live/dead cell staining using mouse fibroblast NIH3T3 cells (RIKEN BioResource Research Center, Japan). For cell culture, we used a medium (MEM alpha, GlutaMAX-I, Thermo Fisher Scientific, USA) supplemented with 10% fetal bovine

serum (Thermo Fisher Scientific) and 1% penicillin-streptomycin (Thermo Fisher Scientific). Sample RC was used as a control.

For the cell proliferation assay, the disk-shaped specimens of Samples RC (control) and A-RC prepared in Section 2.3 were placed in a 96-well cell culture plate (one specimen per well). The cells were seeded (1×10^4 cells/0.2 mL/well) and cultured on the specimen in a humidified atmosphere with 5% CO_2 at 37°C. After culturing for various periods up to 7 d, the cell number in each well was assayed with water-soluble tetrazolium salt-8 using a cell counting kit (CCK-8; Dojindo Laboratories, Mashiki, Japan) according to the manufacturer's instructions. The absorbance was measured at 450 nm using a microplate reader (Multiskan™ FC, Thermo Fisher Scientific).

For actin and live/dead cell staining, the cells were cultured for 1 d using the same protocol previously described except for the culture plate (48-well cell culture plate) and seeding condition (1×10^4 cells/0.3 mL/well). For actin staining, the cells after culturing were washed with phosphate-buffered saline (PBS), fixed with 4% paraformaldehyde phosphate buffer solution (FUJIFILM Wako Pure Chemical Corp., Japan), and stained for actin with 80 nM fluorescent phalloidin (Acti-stain 555 fluorescent Phalloidin, Cytoskeleton Inc., USA). For live/dead cell staining, the cells after culturing were washed with PBS and stained for live cells and dead cell nuclei, respectively, with 2 μM calcein-AM and 4 μM ethidium homodimer-1 using a LIVE/DEAD® Viability/Cytotoxicity kit for mammalian cells (Thermo Fisher Scientific). The stained cells were observed using a fluorescence microscope (BZ-9000 BioRevo, Keyence Corporation, Japan). In the captured images, the stained regions were quantified using an image processing program (Image J, 1.41, National Institutes of Health, Bethesda, USA).

In the cell proliferation and live/dead cell staining assays, 7 and 3 specimens were

tested, respectively, for each sample. The results were analyzed using Student's *t*-test, and $p < 0.05$ was considered statistically significant.

3. Results and Discussion

3.1 Surface analyses of the as-prepared apatite-coated PET film

We confirmed that an apatite-coated PET film was prepared *via* the precursor-assisted biomimetic process, as reported previously [22]. As shown in the SEM image in Figure 2a, a micro-rough layer consisting of randomly oriented micro-flakes was observed on the PET surface after the process. The micro-rough layer was apparently homogeneous and covered the entire surface (plasma-treated side) of the PET film. According to its EDX spectrum (Figure 2b) and thin-film XRD profile (Figure 2c), this micro-rough layer was composed mainly of O, P, and Ca, and contained low-crystallinity hydroxyapatite as a major crystalline phase. These results suggest that the PET film was fully coated with a micro-rough apatite layer by the present process. The content of apatite in the apatite-coated PET film was estimated to be 10.3 ± 1.5 vol% according to the layer thickness (determined by cross-sectional SEM analysis in Section 3.3).

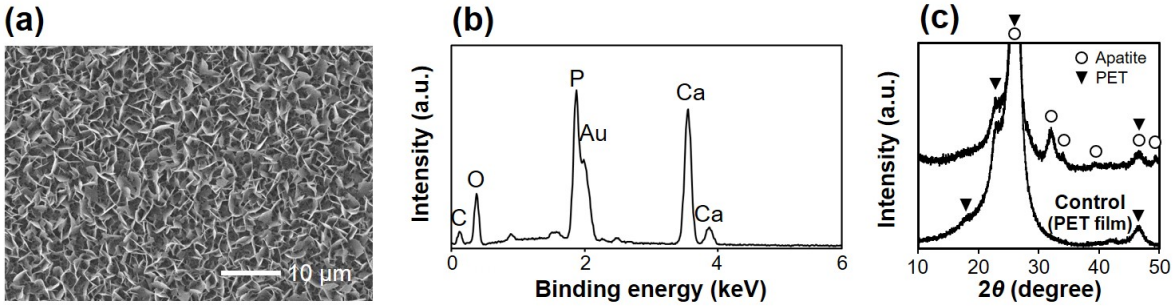

Fig. 2 (a) SEM image, (b) EDX spectrum, and (c) thin-film XRD profile (measured with Ultima III) of the surface of the apatite-coated PET film. Control in (c) is the thin-film XRD profile of the surface of the uncoated PET film.

3.2 Surface analyses of the apatite-coated PET film after use in Sample A-RC preparation

Part of the apatite layer on the PET film was removed by the cured resin composite. We analyzed the surface of the apatite-coated PET films after they were used in the preparation of Sample A-RC, *i.e.*, after the film was peeled from the cured resin composite. As shown in the SEM images (Figure 3a) and the corresponding EDX spectra (Figure 3b), the surface morphology and composition varied greatly depending on the region: (i) the outer region, (ii) the central circular region (⌀5 mm) detached from the cured resin composite, and (iii) the circumference of region (ii). On the outer region (i), we observed a remaining apatite layer with a morphology and composition similar to those of the as-prepared apatite-coated PET film [compare Figures 2 and 3(i)]. By contrast, no such layer was observed on the central circular region (ii); the surface was fairly smooth and composed of C and O, which are component elements of PET. Neither P nor Ca was detected in this region by EDX. These results indicate that the apatite layer in the central circular region (ii) was detached from the PET surface, whereas that on the outer region (i) remained intact, after the PET film was peeled from the cured resin composite. On the circumference (iii) of the circular region (ii), a micro-powdery layer consisting of O, Al, Si, and Ba was found spread over the remaining apatite layer. Given the particle size (~0.7 μm in diameter) and composition of these micro-powders, they should be SiO_2–BaO-based glass fillers in the resin composite. We considered that the resin composite precursor was extruded from the mold cavity during press molding followed by light-induced curing at the interstices between the mold top-face and the apatite-coated PET

film.

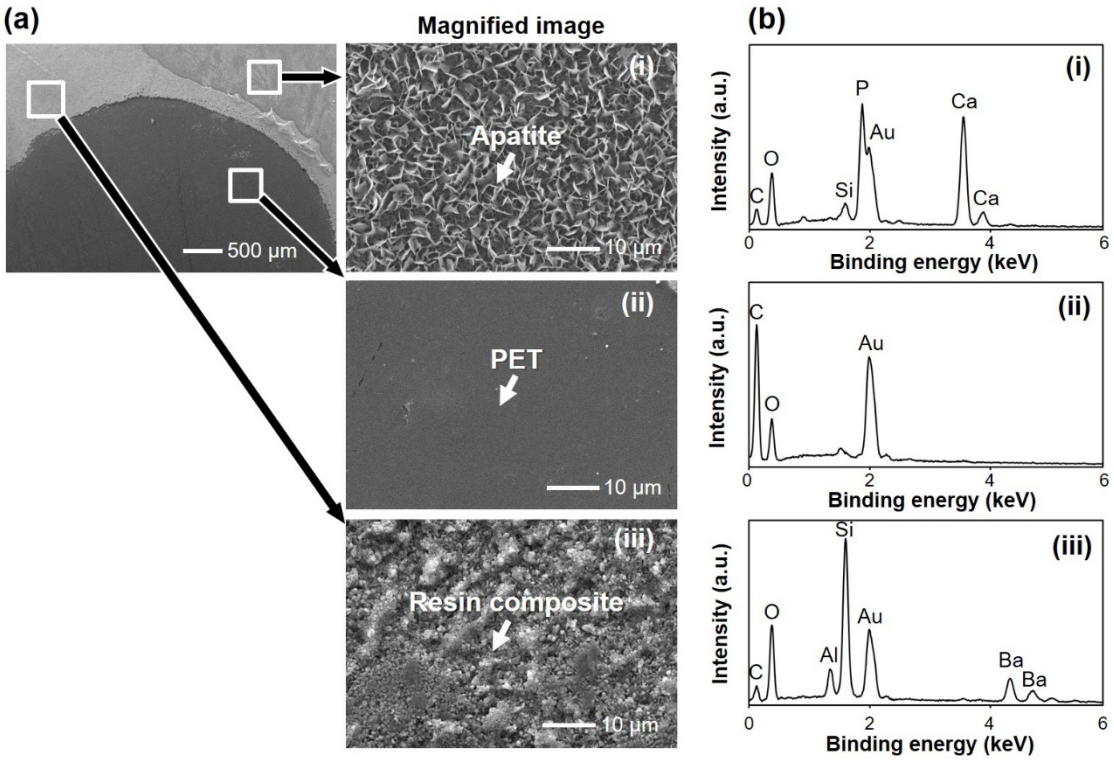

Fig. 3 (a) SEM images in lower (left) and higher (right) magnifications and (b) EDX spectra of the surface of the apatite-coated PET film after the specimen was used for the preparation of Sample A-RC: (i) outer region, (ii) central circular region (⌀5 mm) detached from the cured resin composite, and (iii) circumference of region (ii).

3.3 Surface analyses of Sample A-RC

The apatite-coated resin composite was successfully prepared by light-induced curing in conjunction with the use of the apatite-coated PET film. As shown in the SEM images in Figure 4a, Sample A-RC (lower row) had a dense and flat surface, different from the micro-powdery surface of Sample RC (upper row). The RC surface contained numerous SiO_2–BaO-based glass fillers, as suggested by the SEM and EDX results in Figure 4 (upper row). By contrast, the A-RC surface was composed of CaP, because P and

Ca were detected as major component elements by EDX (refer to the lower EDX spectrum in Figure 4b). This result suggests the presence of a top CaP layer on Sample A-RC. The top CaP layer was identified as low-crystallinity hydroxyapatite because the XRD pattern for Sample A-RC showed broad diffraction peaks characteristic of hydroxyapatite (Figure 5). The resin composite itself did not contain any crystalline phase, as indicated by the XRD pattern for Sample RC. Given the results shown in Figure 3, the apatite layer found on the A-RC surface should be transferred from the apatite-coated PET film as a result of resin curing. The apatite layer on Sample A-RC (Figure 4a, lower row) was completely different in surface morphology from the source apatite layer on the PET film (Figure 2a). This difference in morphology is attributed to the micro-rough apatite layer on the PET film being flipped upside down when transferred onto the cured resin composite (see Figure 1), leading to the exposure of the flat surface initially attached to the PET surface.

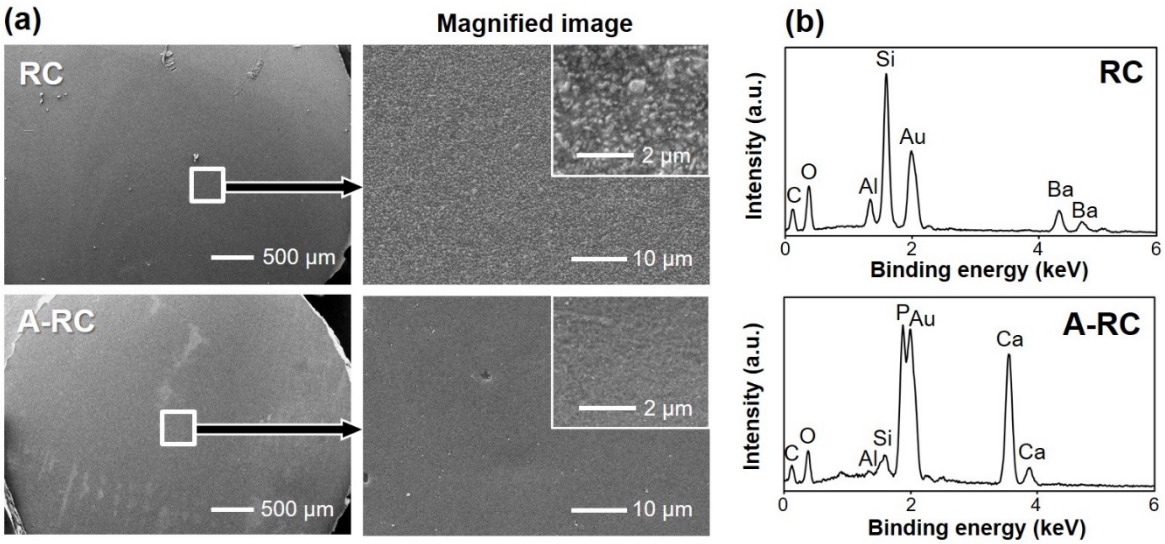

Fig. 4 (a) SEM images in lower (left) and higher (right) magnifications and (b) EDX spectra of the surfaces of Samples RC (upper row) and A-RC (lower row). Insets in (a) are higher-magnification images.

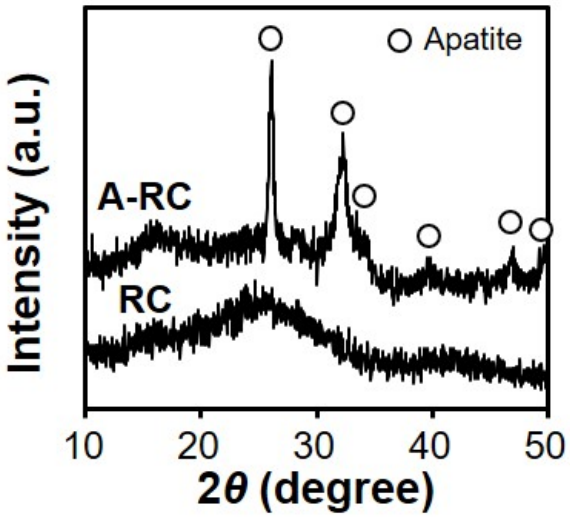

Fig. 5 Thin-film XRD profiles (measured with Ultima IV) of the surfaces of Samples RC and A-RC.

The surface apatite layer attached directly to the cured resin composite without any gaps at the microscopic level. Figure 6a shows cross-sectional SEM images of the A-RC surface. The locations of apatite and the resin composite in the magnified SEM image were visualized by the corresponding EDX mapping images of Si and Ca, respectively (Figure 6b). The lower-magnification SEM image in Figure 6a shows that the apatite layer covered the entire surface of the resin composite. The thickness of the apatite layer was 2.7 ± 0.4 μm. In the magnified SEM image, no structural defects such as voids or cracks are observed at the interface between the apatite layer and the resin composite. Notably, the interface between them was jagged, most likely because of the micro-rough morphology of the apatite layer (see Figure 2a).

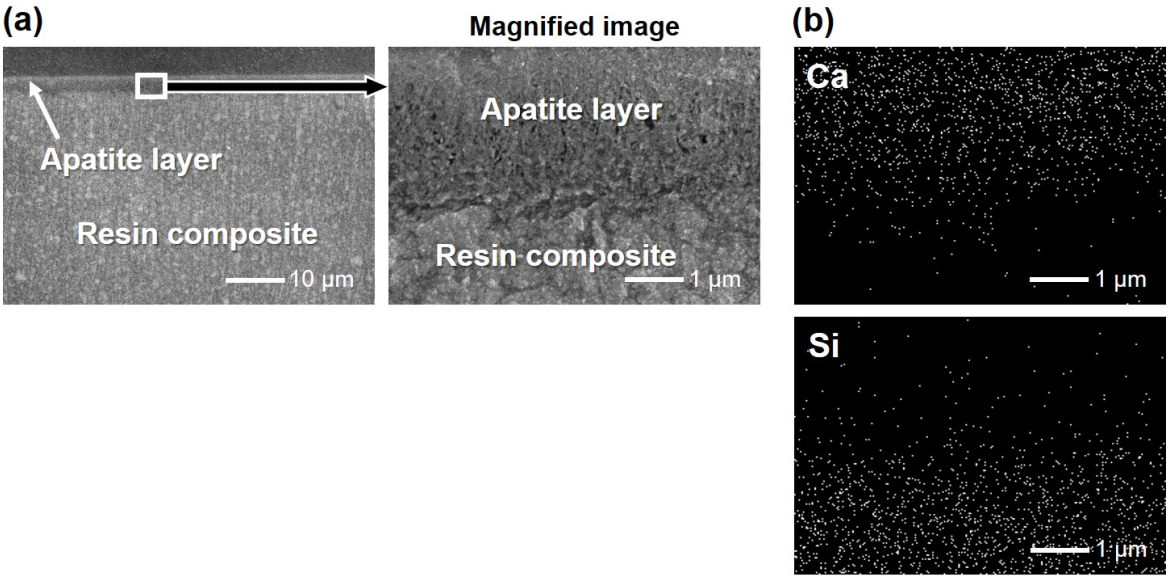

Fig. 6 (a) SEM images in lower (left) and higher (right) magnifications and (b) EDX elemental (Ca, Si) mapping images of the cross-sectional surface of Sample A-RC.

3.4 Mechanism of apatite coating on Sample A-RC

As described above, apatite coating of the resin composite was completed simultaneously with light curing of the resin composite through the apatite-coated PET film (scheme shown in Figure 1). The apatite coating mechanism can be described as follows. In the proposed technique, the apatite-coated PET film (Figure 2) was used to cover the resin composite precursor injected into the mold. During mold pressing, the low-viscosity precursor spread throughout the cavity and filled the gap with the micro-rough apatite layer, as is evident in the cross-sectional SEM images (Figure 6). At the same time, the surplus precursor was extruded to the circumference of the mold cavity (to the interstices between the mold top-face and the apatite-coated film). This situation is illustrated schematically in Figure 7a. The precursor pressed under the apatite-coated PET film was then cured by light irradiated through the film. When the PET film was subsequently detached from the cured resin composite, interfacial peeling fracture

occurred not at the resin–apatite interface but at the PET–apatite interface [see Figures 3(ii) and 7b]. In the circumference of this central circular region, interfacial peeling fracture occurred not at the resin–apatite interface but at the mold–resin interface [see Figures 3(iii) and 7b]. These interfacial peeling fracture modes indicate stronger adhesion at the resin–apatite interface than at the PET–apatite and mold–resin interfaces. The thus-obtained resin composite (Sample A-RC) had a dense and flat apatite layer on its surface (Figures 4–6). In summary, in the present coating technique, the apatite layer was transferred from the PET film onto the cured resin composite surface as a result of the difference in interfacial adhesion strength (PET–apatite < resin–apatite).

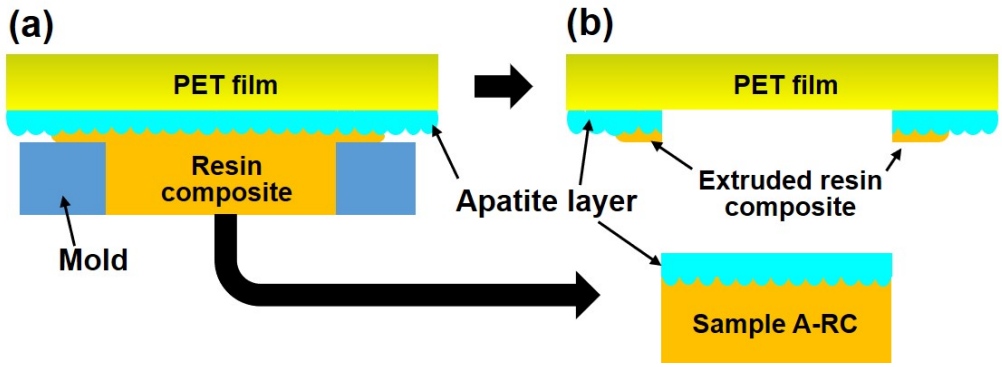

Fig. 7 Schematics of (a) the resin composite cured through attachment of an apatite-coated PET film and (b) its interfacial peeling mode with detachment of the film from the cured resin composite (Sample A-RC).

3.5 Adhesion of apatite coating on Sample A-RC

The apatite layer adhered to the cured resin composite so strongly that it was not peeled off even during the tape-detaching test. We performed the tape-detaching test for Sample A-RC as a preliminary assessment of coating adhesion. The SEM and EDX

analyses show that the apatite layer formed on the A-RC surface remained intact even after the tape-detaching test (Figure 8). In our previous study, the adhesion strength between a PET substrate and the apatite layer prepared by the same coating process was as high as approximately 4 MPa [22]. Even stronger adhesion is expected for the resin–apatite interface in Sample A-RC because of the aforementioned fracture mode of interfacial peeling (Figure 7b). The relatively strong adhesion at the resin–apatite interface might be attributable to the mechanical interlocking effect of the micro-rough apatite layer. Further studies are needed to quantify the adhesion strength between the apatite layer and the resin composite and their bonding mechanism.

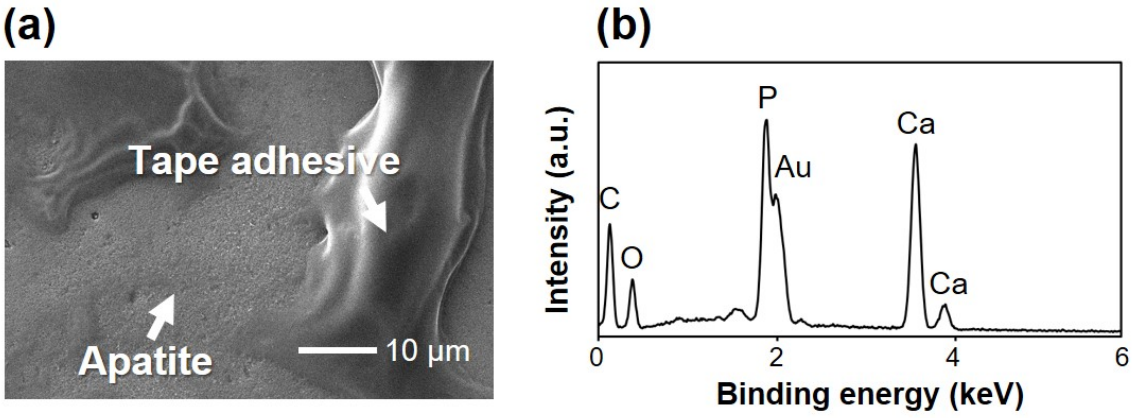

Fig. 8 (a) SEM image and (b) EDX spectrum of the surface of Sample A-RC after the tape-detaching test.

3.6 Molecular structure and flexural strength of A-RC

The resin composite was cured and hardened even in the presence of the apatite layer in the optical path (see the preparation scheme of Sample A-RC in Figure 1). The backside surfaces of Sample A-RC (uncoated side) and Sample RC as a control were analyzed by FT-IR spectroscopy to examine the polymer structure of the cured resin composite. As

shown in Figure 9a, IR peaks at 1453, 1509, 1606, and 1721 cm^{-1} were detected for both samples. These peaks are ascribed to CH_3 bond, N–H/C–N (amide II) and aromatic C=C bonds, aromatic C=C bond, and C=O bond, respectively, from the polymer main chains [26-28]. There was no noticeable difference in either peak position or intensity between Samples RC and A-RC. A small IR peak at 1635 cm^{-1} can be ascribed to aliphatic C=C bonds specific to the non-polymerized monomers carrying terminal double bonds [29]. This C=C peak from residual monomers was detected with similar intensity (with respect to other peaks) for both Samples RC and A-RC. Similar FT-IR results were obtained from three independent measurements with three specimens for each sample. These results suggest that the amount of the unreacted monomers in the cured resin composites was comparable irrespective of the presence of the apatite layer in the optical path. The low blue-light absorption of apatite [25] and the layer's thinness (a few micrometers, as shown in Figure 6a) are likely responsible for the retention of sufficient transmitted light energy for inducing polymerization. The curing light may reduce its energy and penetration depth in the resin composite precursor by passing through the apatite layer, thereby affecting the degree of polymerization, although such an effect was not observed under the investigated experimental conditions.

The flexural strength of the apatite-coated resin composite was comparable to that of the resin composite without a coating. Figure 9b shows the flexural strengths of Samples RC (control) and A-RC. Both samples satisfied the requirement for flexural strength (80 MPa) of polymer-based restorative materials specified in standard ISO 4049 [24]. No significant difference in flexural strength was observed between the two samples ($p > 0.05$). In the three-point bending test, fracture starts at the bottom surface (tension side) of the specimen. Thus, the flexural strength of resin composites is affected by their surface

characteristics [30, 31]. Despite the presence of the weak and brittle apatite layer on the specimen surface, no significant decrease was observed in the flexural strength of Sample A-RC compared to that of Sample RC ($p > 0.05$). This similar flexural strength suggests that the surface apatite layer does not significantly affect the flexural strength of the underlying bulk resin composite.

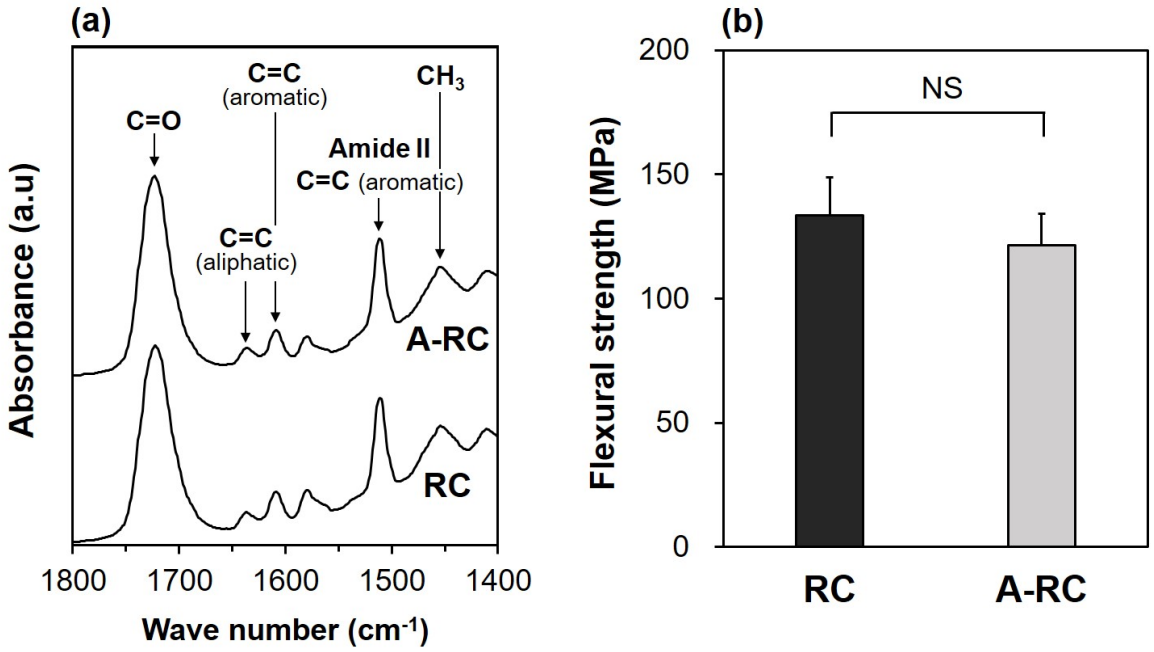

Fig. 9 (a) FT-IR spectra of the backside surfaces and (b) flexural strengths (n = 6, mean + standard deviation, NS: $p > 0.05$) of Samples RC and A-RC.

3.7 Cell compatibility of A-RC

The apatite-coated resin composite exhibited better cell compatibility than the uncoated resin composite. Figure 10 shows the relative number of cells after culturing for 1, 3, 5, and 7 days on the RC (control) and A-RC surfaces. On both samples, the number of cells increased with increasing culturing period *via* proliferation. The number of cells was comparable ($p > 0.05$) for Samples RC and A-RC during the initial stage of culture up to 5 d. However, after 7 d of culturing, the number of cells became significantly larger

for Sample A-RC than for Sample RC ($p < 0.05$). This result indicates that the cells proliferated faster on Sample A-RC than on Sample RC. The cells after culturing for 1 d were examined by actin and live/dead cell staining assays. The actin staining assay indicated that the cells on the A-RC surface exhibited enhanced adhesion and spreading compared with those on the RC surface (Figure 11a). The live/dead cell staining assay revealed that the cells cultured on the RC surface apparently included a larger number of dead cells (represented in red) than those on the A-RC surface (Figure 11b). This observation was confirmed by the quantitative results showing that the rate of the green-stained region (representing live cells) was higher for Sample A-RC than for Sample RC, whereas that of the red-stained region (representing dead cell nuclei) showed the opposite trend (Figure 11c). These results indicate greater viability of the cells cultured on Sample A-RC. The superior cell compatibility of Sample A-RC compared with that of Sample RC is attributable to the surface apatite layer. Apatite is well known for its excellent protein adsorption capability [32]. For instance, an apatite layer formed in the same CP solution shows high affinity with cell adhesion proteins such as fibronectin [33] and laminin [23]. Thus, enhanced adsorption of cell adhesion proteins might be involved in the improved cell adhesion, proliferation, and viability on the A-RC surface through the surface apatite layer. A blocking effect of the apatite layer for the release of residual monomers from the cured resin composite might also have contributed to the improved cell compatibility of Sample A-RC.

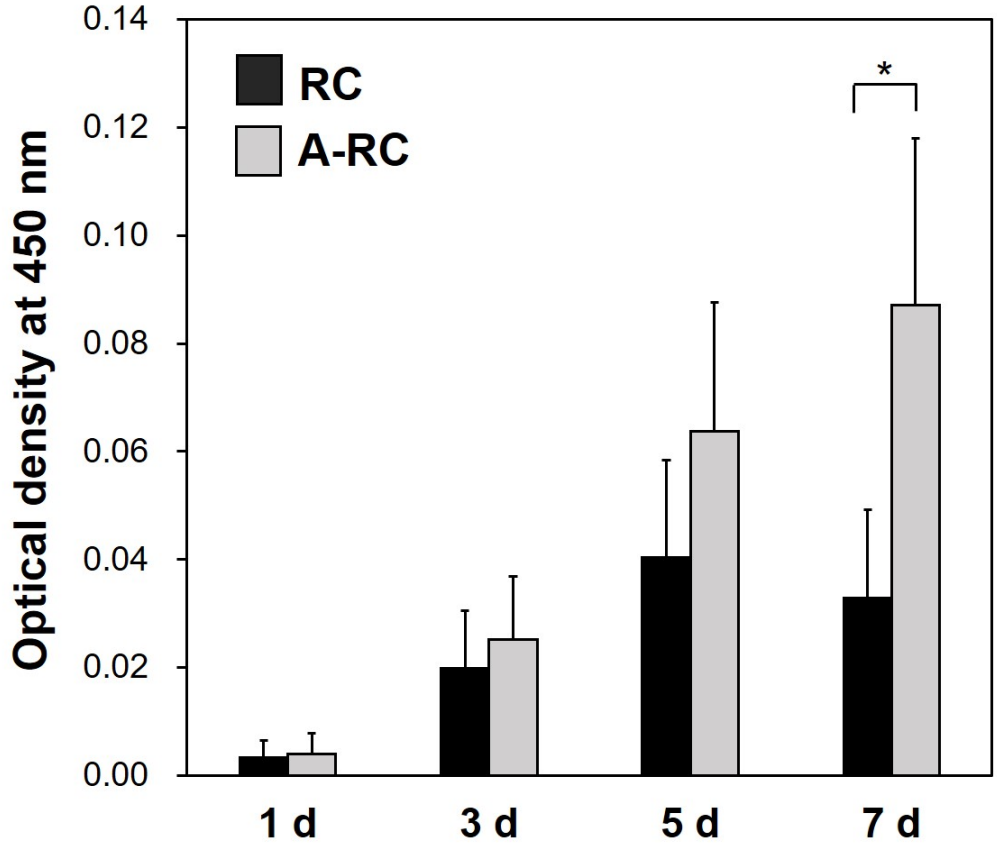

Fig. 10 Relative number of NIH3T3 cells (optical density at 450 nm) after culturing on Samples RC and A-RC for 1, 3, 5, and 7 d (*n* = 7, mean + standard deviation, *: $p < 0.05$).

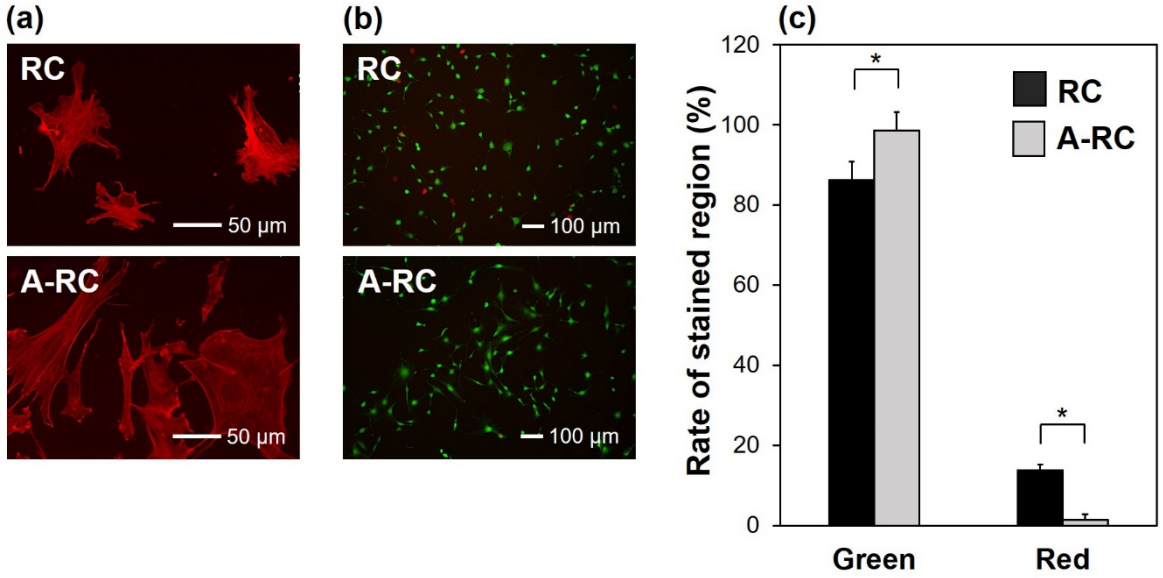

Fig. 11 (a,b) Fluorescence microscopic images of the stained cells cultured for 1 d on Samples RC and A-RC after (a) actin staining and (b) live/dead cell staining. (c) Rate of green- and red-stained regions in the fluorescence microscopic images after live/dead cell staining (n = 3, mean ± standard deviation, *: $p < 0.05$). Red-stained region in (a) represents actin fibers, and green- and red-stained regions in (b,c) represent live cells and dead cell nuclei, respectively.

3.8 Perspectives

We achieved apatite coating on the resin composite just by employing a PET film coated with a micro-rough apatite layer in a conventional light-curing procedure (Figure 1). A similar polymer film (with no coating) has already been used as a dental strip for the preparation of light-curing resin composites for interproximal and cervical restoration. Apatite has also been used in various implantable biomaterials for more than three decades [16, 17]. Therefore, the apatite-coated PET film is well suited as a biomaterial

for dental applications. The proposed apatite coating technique is potentially available as a standard chair-side treatment procedure without increasing the treatment time or the number of steps and without requiring additional instruments other than a dental curing light. This simplicity is a noteworthy advantage of the present technique over the majority of currently available apatite coating techniques including plasma spraying, sputtering, and pulsed laser deposition [16, 17].

The light-induced curing reaction (light-induced polymerization) occurred even with the use of the apatite-coated PET film in the optical path. In the FT-IR measurements, there was no noticeable effect of the apatite layer on polymer structure of the resulting apatite-coated resin composite (Figure 9a). The apatite-coated resin composite exhibited a flexural strength as high as that of the clinically used dental resin composite (without coating) (Figure 9b), and satisfied the ISO requirement for polymer-based restorative materials in dentistry [24]. The surface apatite layer attached to the cured resin composite without any gaps at a microscopic level (Figure 6) and showed good adhesion according to a preliminary tape-detaching test (Figure 8). The apatite-coated resin composite is expected to exhibit improved biocompatibility with the periodontal tissues owing to the intrinsic biological nature of apatite [16, 17]. This hypothesis is supported by the previous reports [19, 34] and the present *in vitro* results showing that the adhesion and proliferation of mouse fibroblastic NIH3T3 cells were enhanced by the apatite layer coated on the resin composite (Figure 10). According to previously reported *in vivo* results, an apatite layer formed in the same CP solution exhibits good biocompatibility with the living epithelial tissue [34]. In addition, an apatite layer can potentially be loaded with therapeutic agents (e.g., proteins, nucleic acids, or trace elements) by adding these agents to the CP solution [21, 35]. An apatite layer loaded with fibroblast growth factor-2 is reported to enhance

wound healing associated with Sharpeys fiber-like tissue formation around a percutaneous implant in rabbits [36]. For the aforementioned reasons, the present apatite coating technique has the potential in dental restoration to repair a damaged tooth root surface via light-curing resin composites. Topics for future studies include optimization of the layer's thickness, microstructure, crystal structure, and composition with regard to adhesion and chemical durability of the coating, along with an *in vivo* evaluation of the periodontal tissue response to the apatite-coated resin composite.

4. Conclusion

We developed a simple technique for coating apatite onto a resin composite using just a PET film coated with a micro-rough apatite layer in the conventional light-curing procedure. During light-curing, the micro-rough apatite layer was transferred from the PET film to the cured resin composite surface because of the difference in interfacial adhesion strength. The transferred apatite layer attached directly and firmly to the cured resin composite without any gaps at the microscopic level. The apatite-coated resin composite was comparable in polymer structure (from the FT-IR results) and flexural strength to the clinically used resin composite. The apatite-coated resin composite showed better cell compatibility than the resin composite without the coating. The present apatite coating technique is safe, easy to use, and offers a potential innovative dental treatment based on light-curing resin composites.

Acknowledgement

The authors acknowledge Ms. Hiroko Araki of the Nanomaterials Research Institute, National Institute of Advanced Industrial Science and Technology (AIST), Japan for

technical support and Dr. Takeyuki Uchida of TIA EM-facility, AIST for cross-sectional sample preparation.

This research did not receive any specific grant from funding agencies in the public, commercial, or not-for-profit sectors.

References

[1] J.L. Ferracane, Resin composite-State of the art, Dent. Mater., 27 (2011) 29-38.

[2] J. Rud, E.C. Munksgaard, J.O. Andreason, V. Rud, E. Asmussen. Retrograde root filling with composite and a dentin-bonding agent 1, Endont. Dent. Traumatol., 7 (1991) 118-125.

[3] M. Trope, C. Lost, H.J. Schmitz, S. Friedman, Healing of apical periodontitis in dogs after apicoectomy and retrofilling with various filling materials, Oral. Surg. Oral. Med. Oral. Pathol. Oral. Radiol. Endod., 81 (1996) 221-228.

[4] S. Imazato, T. Kohno, R. Tsuboi, P. Thongthai, H. H. K. Xu, H. Kitagawa, Cutting-edge filler technologies to release bio-active components for restorative and preventive dentistry, Dent. Mater. J., 39 (2020) 69-79.

[5] J.M. Antonucci, D.N. Zeiger, K. Tang, S. Lin-Gibson, B.O. Fowler, N.J. Lin, Synthesis and characterization of dimethacrylates containing quaternary ammonium functionalities for dental applications, Dent. Mater., 28 (2012) 219-228.

[6] X. Liang, Q. Huang, F. Liu, J. He, Z. Lin, Synthesis of novel antibacterial monomers (UDMQA) and their potential application in dental resin, J. Appl. Polym. Sci., 129 (2013) 3373-3381.

[7] P. Makvandi, M. Ghaemy, M. Mohseni, Synthesis and characterization of photo-curable bis-quaternary ammonium dimethacrylate with antimicrobial activity for dental restoration materials, Eur. Polym. J., 74 (2016) 81-90.

[8] N. Zaltsman, A.C. Ionescu, E.I. Weiss, E. Brambilla, S. Beyth, N. Beyth, Surface-modified nanoparticles as anti-biofilm filler for dental polymers, PLoS One, 12 (2017) e0189397.

[9] M.Z. Kassaee, A. Akhavan, N. Sheikh, A. Sodagar, Antibacterial effects of a new

dental acrylic resin containing silver nanoparticles, J. Appl. Polym. Sci. 110 (2008) 1699-1703.

[10] B.A. Sevinç, L. Hanley, Antibacterial activity of dental composites containing zinc oxide nanoparticles, J. Biomed. Mater. Res. B Appl Biomater. 94B (2010) 22-31.

[11] C. Santos, Z.B. Luklinska, R. L. Clarke, K.W.M. Davy, Hydroxyapatite as a filler for dental composite materials: mechanical properties and *in vitro* bioactivity of composites, J. Mater. Sci.: Mater. Med., 12 (2001) 565-573.

[12] F. Liu, X. Jiang, Q. Zhange, M. Zhu, Strong and bioactive dental resin composite containing poly (Bis-GMA) grafted hydroxyapatite whiskers and silica nanoparticles, Compos. Sci. Technol., 101 (2014) 86-93.

[13] E. Gentleman, Y.C. Fredholm, G. Jell, N. Lotfibakhshaiesh, M.D. O'Donnell, R.G. Hill, M.M. Stevens, The effects of strontium-substituted bioactive glasses on osteoblasts and osteoclasts *in vitro*, Biomater., 31 (2010) 3949-3956.

[14] R. Tsuboi, J. I. Sasaki, H. Kitagawa, I. Yoshimoto, F. Takeshige, S. Imazato, Development of a novel dental resin cement incorporating FGF-2-loaded polymer particles with the ability to promote tissue regeneration. Dent. Mater., 34 (2018) 641-648.

[15] A.J. Nathanael, A. Oyane, M. Nakamura, K. Koga, E. Nishida, S. Tanaka, H. Miyaji, Calcium phosphate coating on dental composite resins by a laser-assisted biomimetic process, Heliyon., 4 (2018) e00734.

[16] K. Pajor, L. Pajchel, J. Kolmas, Hydroxyapatite and fluorapatite in conservative dentistry and oral implantology—A review, Materials, 12 (2019) 2683.

[17] A. Haider, S. Haider, S.S. Han, I-K. Kang, Recent advances in the synthesis, functionalization and biomedical applications of hydroxyapatite: a review, RSC Adv., 7 (2017) 7442-7458.

[18] L. Mao, J. Liu, J. Zhao, J. Chang, L. Xia, L. Jiang, X. Wang, K. Lin, B. Fang, Effect of micro-nano-hybrid structured hydroxyapatite bioceramics on osteogenic and cementogenic differentiation of human periodontal ligament stem cell via Wnt signaling pathway, Int. J. Nanomedicine, 10 (2015) 7031-7044.

[19] T. Kano, R. Yamamoto, A. Miyashita, K. Komatsu, T. Hayakawa, M. Sato, S. Oida, Regeneration of periodontal ligament for apatite-coated tooth-shaped titanium implants with and without occlusion using rat molar model, J. Hard. Tissue. Biol., 21 (2012) 189-202.

[20] M. Oshima, K. Inoue, K. Nakajima, T. Tachikawa, H. Yamazaki, T. Isobe, A. Sugawara, M. Ogawa, C. Tanaka, M. Saito, S. Kasugai, T. Takano-Yamamoto, T. Inoue, K. Tezuka, T. Kuboki, A. Yamaguchi, T. Tsuji, Functional tooth restoration by next-generation bio-hybrid implant as a bio-hybrid artificial organ replacement therapy, Sci. Rep., 4 (2015) 6044.

[21] A. Oyane, X.P. Wang, Y. Sogo, A. Ito, H. Tsurushima, Calcium phosphate composite layers for surface-mediated gene transfer, Acta Biomater., 8 (2012) 2034-2046.

[22] H. Mutsuzaki, Y. Yokoyama, A. Ito, A. Oyane, Formation of apatite coatings on an artificial ligament using a plasma- and precursor-assisted biomimetic process, Inter. J. Mol. Sci., 14 (2013) 19155-19168.

[23] M. Uchida, A. Oyane, H.M. Kim, T. Kokubo, A. Ito, Biomimetic coating of laminin-apatite composite on titanium metal and its excellent cell-adhesive properties, Adv. Mater., 16 (2004) 1071-1074.

[24] ISO 4049: 2019. Dentistry-Polymer-based restorative materials, International Organization for Standardization.

[25] A.J. Nathanael, A. Oyane, M. Nakamura, M. Mahanti, K. Koga, K. Shitomi, H.

Miyaji, Rapid and area-specific coating of fluoride-incorporated apatite layers by a laser-assisted biomimetic process for tooth surface functionalization, Acta Biomater., 79 (2018) 148-157.

[26] R.M. Guerra, I. Durán, P. Ortiz, Chapter 4 FTIR monomer conversion analysis of dental resins, in: G.E. Zaikov, A. Jiménez (Eds.), Chemical Reactions: Quantitative Level of Liquid and Solid Phase, Nova Science Publishers Inc., New York, 2004, pp.59-74.

[27] J.M. Antonucci, S.H. Dickens, B.O. Fowler, H.H.K. Xu, W.G. McDonough, Chemistry of silanes: Interfaces in dental polymers and composites, J. Res. Natl. Inst. Stand. Technol., 110 (2005) 541-558.

[28] G. Duan, C. Zhang, A. Li, X. Yang, L. Lu, X. Wang, Preparation and characterization of mesoporous zirconia made by using a poly (methyl methacrylate) template, Nanoscale. Res. Lett. 3 (2008) 118-122.

[29] A.B. Denis, C.A. Diagone, A.M.G. Plepis, R.B. Viana, Kinetic parameters during Bis-GMA and TEGDMA monomer polymerization by ATR-FTIR: the influence of photoinitiator and light curing source, J. Spectrosc., 2016 (2016) article ID 6524901.

[30] U. Lohbauer, F.A. Müller, A. Petschelt, Influence of surface roughness on mechanical strength of resin composite versus glass ceramic materials, Dent. Mater., 24 (2008) 250-256.

[31] S. Flury, A. Peutzfeldt, A. Lussi, Influence of surface roughness on mechanical properties of two computer-aided design/computer-aided manufacturing (CAD/CAM) ceramic materials, Oper. Dent., 37 (2012) 617-624.

[32] L.J. Cummings, M.A. Snyder, K. Brisack, Protein chromatography on hydroxyapatite columns, Methods in Enzymology, 463 (2009) 387-404.

[33] A. Oyane, M. Murayama, A. Yamazaki, Y. Sogo, A. Ito, H. Tsurushima, Fibronectin-DNA-apatite composite layer for highly efficient and area-specific gene transfer, J. Biomed. Mater. Res., A 92 (2010) 1038-1047.

[34] K. Sasaki, A. Oyane, K. Hyodo, A. Ito, Y. Sogo, M. Kamitakahara, K. Ioku, Preparation and biological evaluation of a fibroblast growth factor-2–apatite composite layer on polymeric material, Biomed. Mater., 5 (2010) 065008-065017.

[35] X.P. Wang, A. Oyane, A. Ito, Signal molecule-calcium phosphate composites: Novel approaches to controlling cellular and/or biological reactions and functions, in: B. Ben-Nissan (Ed.), Advances in Calcium Phosphate Biomaterials, Springer Series in Biomaterials Science and Engineering 2, Springer Link, Switzerland, 2014, pp. 171-197.

[36] H. Mutsuzaki, A. Ito, Y. Sogo, M. Sakane, A. Oyane, N. Ochiai, Enhanced wound healing associated with Sharpeys fiber-like tissue formation around FGF-2-apatite composite layers on percutaneous titanium screws in rabbits, Arch. Orthop. Trauma. Surg., 132 (2012) 113-121.